The Astrophysical Journal, 686:1195–1208, 2008 October 20

A *SPITZER* VIEW OF PROTOPLANETARY DISKS IN THE γ VELORUM CLUSTER

Jesús Hernández,[1,2] Lee Hartmann,[1] Nuria Calvet,[1] R. D. Jeffries,[3]
R. Gutermuth,[4] J. Muzerolle,[5] and J. Stauffer[6]
Received 2008 March 3; accepted 2008 June 16

ABSTRACT

We present new *Spitzer Space Telescope* observations of stars in the young ($\sim$5 Myr) γ Velorum stellar cluster. Combining optical and 2MASS photometry, we have selected 579 stars as candidate members of the cluster. With the addition of the *Spitzer* mid-infrared data, we have identified five debris disks around A-type stars and five to six debris disks around solar-type stars, indicating that the strong radiation field in the cluster does not completely suppress the production of planetesimals in the disks of cluster members. However, we find some evidence that the frequency of circumstellar primordial disks is lower, and the infrared flux excesses are smaller than for disks around stellar populations with similar ages. This could be evidence for a relatively fast dissipation of circumstellar dust by the strong radiation field from the highest mass star(s) in the cluster. Another possibility is that γ Velorum stellar cluster is slightly older than reported ages and the low frequency of primordial disks reflects the fast disk dissipation observed at $\sim$5 Myr.

Subject headings: infrared: stars — open clusters and associations: individual (γ Velorum) — planetary systems: protoplanetary disks — stars: pre–main-sequence

Online material: color figures, machine-readable tables

1. INTRODUCTION

In recent years the sensitivity of the *Spitzer Space Telescope* has made it possible to expand our knowledge of dusty disk emission dramatically, enabling statistically significant studies of disk emission as a function of mass and age over a much wider wavelength range than previously possible (e.g., Lada et al. 2006; Sicilia-Aguilar et al. 2006; Hernández et al. 2007a, 2007b). In addition to confirming the rapid decrease of optically thick disk emission previously inferred from near-infrared observations (Strom et al. 1989; Haisch et al. 2001), *Spitzer* observations have provided strong evidence that disk dissipation timescales depend significantly on host star mass (Lada et al. 2006; Carpenter et al. 2006; Hernández et al. 2007a), with a timescale for inner disk dissipation of 5–7 Myr (Haisch et al. 2001; Hartmann 2005; Hernández et al. 2007a) for low-mass stars ($\lesssim 1\ M_\odot$) and $<$3 Myr (Hernández et al. 2005) for intermediate-mass stars (2–10 $M_\odot$). *Spitzer* observations have also provided new clues to disk structure through spectral energy distribution (SED) analysis, from slight indications of faster dust settling in inner disks (Sicilia-Aguilar et al. 2006) to strong evacuation of the inner disks in some stars that retain optically thick outer disks (Calvet et al. 2002, 2005; D'Alessio et al. 2005a; Espaillat et al. 2007b). *Spitzer* data have also been used to show that debris disks around intermediate-mass stars are more frequent and have larger 24 μm excesses around 10–13 Myr, when models predict that dust is produced by collisional cascades due to the formation of large solid bodies ($\sim$1000 km) in the disk (Kenyon & Bromley 2005; Hernández et al. 2006; Currie et al. 2008).

The possible effects of environment on disk frequency and structure are less clear. In clusters with high-mass stars, disk photoevaporation due to the strong ultraviolet radiation field can be important, and it is directly observed in the Orion Nebula Cluster (Richling & Yorke 2000; Adams et al. 2004; Hollenbach & Adams 2004; Throop & Bally 2005; Clarke 2007; Megeath et al. 2007). Balog et al. (2007) found a reduction in disk frequency of about a factor of 2 in the relatively young cluster NGC 2244, but only in the innermost regions ($d \lesssim 0.5$ pc). NGC 2244 is very rich and contains seven O-type stars, so that the ultraviolet radiation field should be very strong.

The discovery of a young cluster of low-mass stars around the γ Vel system (Pozzo et al. 2000), with the central binary consisting of an O 7.5 star and a Wolf-Rayet star (De Marco & Schmutz 1999; De Marco et al. 2000), provides an opportunity to study the possible effects of central star ultraviolet radiation fields on disk evolution. The Wolf-Rayet star is classified as WC8 (carbon-rich), implying a progenitor mass of $>$40 $M_\odot$ (De Marco & Schmutz 1999; Crowther 2007). In this paper we report *Spitzer* observations of infrared emission in this cluster. In § 2 we present the observational data used in this contribution and discuss membership in § 3. We analyze the infrared data in § 4 and compare with disk frequencies in other young stellar populations in § 5, with our main results summarized in § 6.

2. OBSERVATIONS

2.1. *Infrared Photometry*

We have obtained near-infrared (NIR) and mid-infrared photometry of the γ Velorum cluster using the four channels (3.6, 4.5, 5.8, and 8.0 μm) of the Infrared Array Camera (IRAC; Fazio et al. 2004) and the 24 μm band of the Multiband Imaging Spectrometer for *Spitzer* (MIPS; Rieke et al. 2004) on board the *Spitzer Space Telescope*. These data were collected during 2005 February 23 (IRAC) and April 10 (MIPS) as part of a GTO program conducted by the IRAC and MIPS instrument teams.

The IRAC observations were done using a standard raster map with 280″ offsets, to provide maximum areal coverage while still allowing $\sim$20″ overlap between frames in order to facilitate accurate mosaicking of the data. The mapped region was covered

[1] Department of Astronomy, University of Michigan, 830 Dennison Building, 500 Church Street, Ann Arbor, MI 48109.
[2] Centro de Investigaciones de Astronomía, Apdo. Postal 264, Mérida 5101-A, Venezuela.
[3] Astrophysics Group, School of Physical and Geographical Sciences, Keele University, Keele, Staffordshire ST5 5BG, UK.
[4] Harvard-Smithsonian Center for Astrophysics, 60 Garden Street, Cambridge, MA 02138.
[5] Steward Observatory, University of Arizona, 933 North Cherry Avenue, Tucson, AZ 85721.
[6] Spitzer Science Center, Mail Stop 220-6, California Institute of Technology, 1200 East California Boulevard, Pasadena, CA 91125.

by a 9×10 position mosaic, with three dither exposures at each position. Images were obtained in high dynamic range (HDR) mode, in which a short integration (1 s) is immediately followed by a long integration (26.8 s). Standard basic calibrated data (BCD) products from version S14.0.0 of the Spitzer Science Center's IRAC pipeline were used to make the final mosaics. Post-BCD data treatment was performed using custom IDL software (Gutermuth et al. 2004) that includes modules for detection and correction of bright-source artifacts, detection and removal of cosmic-ray hits, construction of the long- and short-exposure HDR mosaics, and the merger of those mosaics to yield the final science images. The final mosaics have a scale of $1.22''$ pixel^{-1}. Point-source detections were carried out individually on each IRAC band using PhotVis (ver. 1.09), an IDL GUI-based photometry visualization tool developed by R. Gutermuth using the DAOPHOT modules ported to IDL as part of the IDL Astronomy User Library (Landsman 1993).

More than 40,000 sources were detected in at least one IRAC band. We extracted the photometry of these objects using the `apphot` package in IRAF, with an aperture radius of $3.7''$ and a background annulus from $3.7''$ to $8.6''$. We adopted zero-point magnitudes for the standard aperture radius ($12''$) and background annulus ($12''$–$22.4''$) of 19.665, 18.928, 16.847, and 17.391 in the [3.6], [4.5], [5.8], and [8.0] bands, respectively. Aperture corrections were made using the values described in IRAC Data Handbook (Reach et al. 2006). Final photometric errors include the uncertainties in the zero-point magnitudes ($\sim$0.03 mag).

MIPS observations were made using medium scan mode with full-array cross-scan overlap, resulting in a total effective exposure time per pointing of 40 s. The images were processed using the MIPS instrument team Data Analysis Tool (DAT), which calibrates the data and applies a distortion correction to each individual exposure before combining it into a final mosaic (Gordon et al. 2005). A second flat correction was also done to each image using a median of all the images in order to correct for dark latents and scattered light background gradients. The second flat correction is determined by creating a median image of all the data in a given scan leg and then dividing each individual image in that scan leg by that median. Bright sources and extended regions are masked out of the data before creation of the median, so the nebulosity seen in the map has a negligible effect on any noise that might be added by the second flat. We obtained point source photometry at 24 μm with IRAF `daophot` point-spread function fitting, using an aperture size of about $5.7''$ and an aperture correction factor of 1.73 derived from the STinyTim PSF model. The aperture size corresponds to the location of the first airy dark ring and was chosen to minimize effects of source crowding and background inhomogeneities. The sources were identified using an IDL photometry routine, based on the IRAF `daophot` package, with a 10 σ cutoff. Any obvious point sources missed by the find routine were added in by hand. The absolute flux calibration uncertainty is $\sim$4% (Engelbracht et al. 2007). The photometric uncertainties are dominated by the background/photon noise. Our final flux measurements are complete down to about 0.8 mJy.

2.2. *Optical Photometry*

CCD photometry was obtained with the 0.9 m telescope at the Cerro Tololo Inter-American Observatory (CTIO) using a Tek 2048×2048 CCD (13.5×13.5 arcmin^2). A region of 0.93×0.95 deg^2 centered on the γ Velorum system was surveyed in BVI_c with short (20, 10, 6 s) and long (300, 120, 60 s) exposure times (more details in Pozzo et al. 2000; R. D. Jeffries et al. 2008, in preparation). Photometry was performed on the reduced data using the optimal extraction algorithm detailed in Naylor (1998) and Naylor et al. (2002). Stars closer than $3'$ to the central object have poor photometry because of the brightness of the γ Velorum system. The optical catalog includes 24,730 sources in the IRAC field ranging from $V = 10$ to 21 and with photometric errors less than 0.1 mag. We augmented the V, B optical data set toward the brightest objects using the Kharchenko (2001) catalog. A preliminary list of 15,712 objects (hereafter sample 1) was created by selecting the optical sources that have photometric measurements in all IRAC bands within $3''$ of matching radius. We have cross-correlated sample 1 with stars in the 2MASS point-source catalog.[7] About 30% of these sources do not have 2MASS counterparts within a $3''$ matching radius; however, many of these objects without a 2MASS counterpart are likely to be background sources (see § 3). In general, optical, 2MASS, and IRAC positions agree within $1''$.

Sample 1 was cross-correlated with the Second *XMM-Newton* Serendipitous Source Catalog (2XMM)[8] using a correlation radius of $3''$, which is the maximum astrometric error expected for most of the sources in 2XMM. In an area of $\sim$0.25 deg^2 around the γ Velorum system about 174 objects in sample 1 have X-ray counterparts.

Finally, 32 stars were confirmed as members of the γ Velorum cluster using the presence of the Li I λ6707 line in absorption, the equivalent width of the Hα line and/or radial velocity in a narrow range around 17 km s^{-1} (Jeffries et al. 2000; R. D. Jeffries et al. 2008, in preparation). The spectroscopic data were obtained at CTIO using the 4 m Blanco telescope in conjunction with the Hydra fiber spectrograph (resolving power $\sim$25,000).

Figure 1 shows the field covered by the optical survey of the γ Velorum cluster. Solid lines indicate the region studied in this paper (IRAC field), which is the area covered by the four IRAC channels and where sample 1 is located. The MIPS observation (*dashed lines*) covers most ($\sim$90%) of this area. The 2XMM catalog covers about 30% of the IRAC field; X-ray sources are indicated on the image (*crosses*). Most of the members confirmed spectroscopically (*open squares*) are X-ray sources. Only three spectroscopic members do not have X-ray counterparts, and they are all located outside the 2XMM field of view. The ringlike diffuse emission structure around the γ Velorum cluster confirms that some of the gas from which the cluster formed is still present.

3. MEMBERSHIP SELECTION

Our membership selection is based on using the sequence defined by the spectroscopic members (Jeffries et al. 2000; R. D. Jeffries et al. 2008, in preparation) and the X-ray sources from 2XMM. As most of the stars in sample 1 do not have spectroscopic data, we use photometric criteria to make a selection of potential members based on their colors and magnitudes. Figure 2 shows color magnitude diagrams (CMDs), V versus $V - J$ (*left panels*) and V versus $V - I$ (*right panels*), illustrating the procedure to select photometric candidates of the γ Velorum cluster. We assume a distance of 350 pc (see § 5) to plot the zero-age main sequence (*solid line*) and the 5 Myr isochrone (*dashed line*) from Siess et al. (2000). Since it is well known that theoretical, nonbirthline isochrones do not accurately match empirical isochrones for intermediate-mass stars (Hartmann 2003) and that the opacity tables at low temperatures are incomplete (Lyra et al. 2006; Baraffe et al. 1998), these theoretical isochrones are plotted as reference only and are not used for the selection of the photometric candidates (however, evidence in favor of this age

[7] Vizier Online Data Catalog, 2246, 0 (R. M. Cutri et al. 2003).
[8] At http://xmmssc-www.star.le.ac.uk/Catalogue/2XMM.

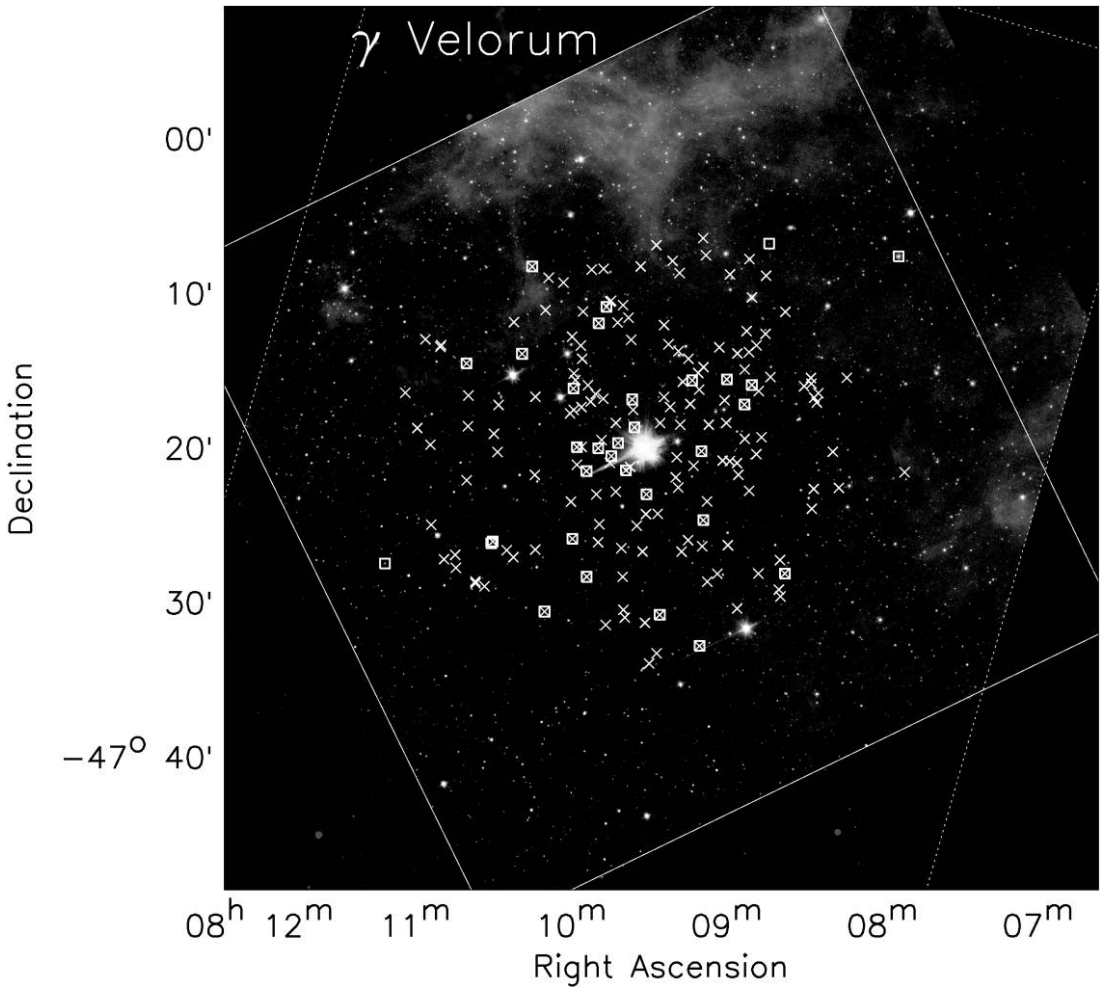

FIG. 1.—False-color image of the γ Velorum cluster. It is a three-color composite of IRAC images: 3.6 μm (*blue*) and 4.5 μm (*green*), and MIPS image, 24 μm (*red*). The plot is centered on the γ Velorum binary system. Solid and dashed lines show the IRAC and MIPS fields, respectively. Members confirmed spectroscopically by R. D. Jeffries et al. (2008, in preparation) are plotted as open squares. Crosses indicate the location of the X-ray sources from the 2XMM catalog. [*See the electronic edition of the Journal for a color version of this figure.*]

is detailed in § 5). Open squares and crosses represent the spectroscopic members and the X-ray sources, respectively. Bright stars with optical photometry from Kharchenko (2001) are plotted as open triangles.

The top left panel shows that X-ray sources are highly concentrated along the nominal empirical isochrone, with a scattering of stars below this region in the CMD probably representing background low-mass stars or other nonmembers. All the spectroscopic members within the 2XMM field are X-ray sources (see Fig. 1). Essentially none of the objects above the nominal isochrone are X-ray sources, and thus are mostly likely heavily reddened giants. In addition, a number of the bright objects from Kharchenko (2001) are also far above the nominal isochrone so we reject them as members as well.

As shown in the top right panel of Figure 2, stars without 2MASS counterparts (*open diamonds*) are located well below the nominal isochrone and even below the ZAMS (at 350 pc), demonstrating that they are background objects.

In the bottom panels we plotted the regions of probable members (*large error bars*). These regions were calculated using the median colors ($V-I$ and $V-J$) of the member sample (spectroscopic members plus X-ray sources above the ZAMS) for 1.0 mag bins in the visual band. We used the differences between the observed colors and the expected colors (the median; *thick solid lines*) to calculate the standard deviation (σ) of the member sample. The regions of probable members are defined using 2.5 σ limit from the median colors (see Hernández et al. 2007a, 2007b). The bottom left panel shows the stars above the ZAMS on the V versus $V-J$ diagram (sample 2), roughly defined using a straight line, while the bottom right panel shows the V versus $V-I$ diagram for the stars selected using the region of probable members in the V versus $V-J$ diagram (sample 3).

Our final list of photometric candidates includes 579 stars located within the probable member region of the CMDs. Using the 5 Myr isochrone (Siess et al. 2000) at 350 pc and a reddening of $A_V = 0.2$, we estimate that we can detect excess at [5.8] and [8.0] with signal-to-noise ratio (S/N) larger than 5 for a star with spectral type M5 or earlier (at [3.5] and [4.5] the corresponding S/N is larger than 40). For MIPS observations, the completeness limit roughly corresponds to spectral type early K (see § 2.1). Table 1 shows the optical, IRAC, and MIPS photometry of the photometric candidates of the γ Velorum cluster. Column (1) shows the internal running identification number in our sample; column (2) provides the 2MASS object name;[9] columns (3), (4), and (5) give the optical magnitudes in the bands B, V, and I_C, respectively; column (6) indicates the reference for the optical data; columns (7), (8), (9), and (10) give the IRAC magnitudes in the

[9] The version of this table in the electronic edition of the journal also includes 2MASS photometry.

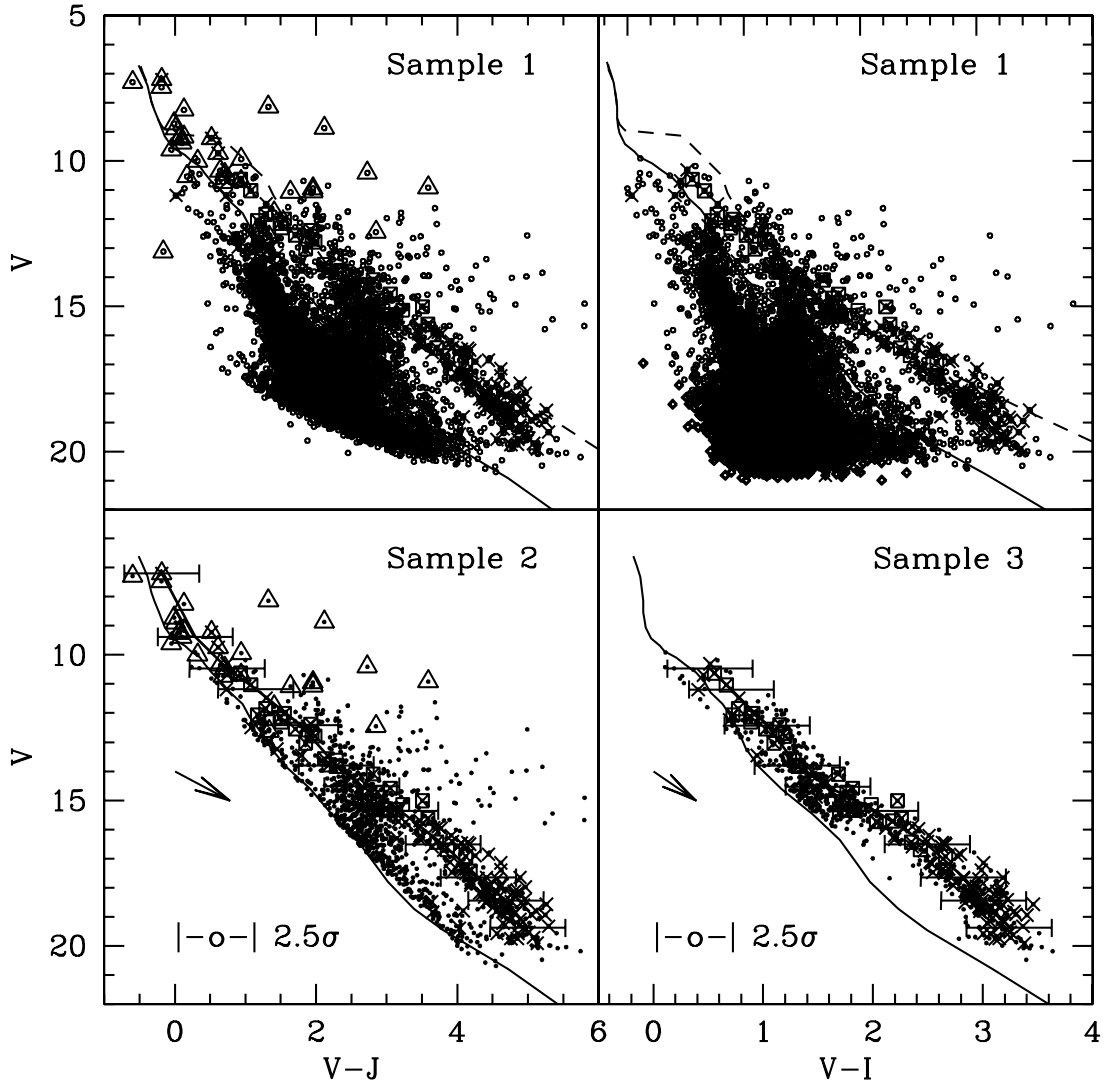

FIG. 2.—Color-magnitude diagrams illustrating the selection of photometric candidates of the γ Velorum cluster. Open squares and crosses represent the spectroscopic members and the X-ray sources, respectively. In the left panels open triangles are stars used to augment the optical data set for the brightest objects (Kharchenko 2001). In the top right panel, open diamonds represent stars without 2MASS counterparts, which are likely background objects. Arrows represent reddening vectors of $A_V = 1$. In the bottom panels big error bars represent the 2.5 σ limits from the median colors (*thick solid line*) of the high-probability member sample; these error bars define the regions used to select the photometric candidates. Assuming a distance of 350 pc, the ZAMS (*solid line*) and the 5 Myr isochrone (*dashed line*) from (Siess et al. 2000) are plotted in the top panels as reference and do not affect the selection of photometric candidates. [*See the electronic edition of the Journal for a color version of this figure.*]

bands [3.6], [4.5], [5.8], and [8.0], respectively; column (11) gives the flux at the 24 μm MIPS band; column (12) indicates whether the star is a 2XMM source; column (13) shows the disk classification based on the IRAC and MIPS analysis (see § 4)

The giant branch of background stars clearly contaminates one portion of the cluster member region defined in Figure 2. We plotted in Figure 3 the V versus $V-J$ diagram for the photometric members illustrating the contamination level expected in several color ranges. Since the reddening of the γ Velorum cluster is quite low ($A_V < 0.2$; Pozzo et al. 2000; R. D. Jeffries 2008, in preparation), we can estimate spectral types for the sources using their $V-J$ color and the standard colors (Kenyon & Hartmann 1995) indicated in the figure. The top panel shows the $V-J$ distributions for the photometric candidates (*open histogram*) and for the spectroscopic or X-ray–selected member sample (*filled histogram*). Within the 2XMM field, more than ~80% of the photometric members with $V-J > 3.5$ are X-ray sources; most stars without X-ray counterparts are very faint ($V > 19.5$) or located near the 2XMM field border. This suggests that most photometric candidates with $V-J > 3.5$ are real members of the γ Velorum cluster. Normalizing the member sample histogram to the photometric candidates histogram in the color range $V-J > 3.5$, we estimate the number of members expected as function of $V-J$ color (*dotted histogram*). The deviation between the expected member distribution and the photometric candidates distribution indicates the level of contamination for a given range of color (or spectral types). The number of photometric candidates increases between $V-J \sim 1.5$ and $V-J \sim 3.5$, where the giant branch crosses the member sequence. In this range of color, the contamination level by nonmembers of the γ Velorum cluster is quite high ($\gtrsim$68%). Since the number of members of stellar groups normally decreases toward higher stellar masses, the relative contamination at $V-J < 1.5$ can still be significant.

Figure 4 shows the 2MASS color color diagram, $J-H$ versus $H-K$, for the photometric members of the γ Velorum cluster. Since the locus of giants separates from main-sequence late-type stars (Bessell & Brett 1988), we can identify background M-type

TABLE 1

MEMBERS OF THE γ VELORUM CLUSTER

ID (1)	2MASS Name (2)	B (mag) (3)	V (mag) (4)	I_C (mag) (5)	Ref. (6)	[3.6] (mag) (7)	[4.5] (mag) (8)	[5.8] (mag) (9)	[8.0] (mag) (10)	$Flux_{24}$ (mJy) (11)	X-Ray Source (12)	Disk Type (13)
1.....	08064389-4731532	19.21 ± 0.02	17.65 ± 0.01	14.98 ± 0.01	1	12.39 ± 0.03	12.38 ± 0.03	12.33 ± 0.04	12.32 ± 0.04	...	0	CIII
2.....	08064805-4728118	13.43 ± 0.01	12.31 ± 0.01	11.15 ± 0.01	1	9.52 ± 0.03	9.57 ± 0.03	9.56 ± 0.03	9.52 ± 0.03	...	0	CIII
3.....	08065006-4732219	19.65 ± 0.03	18.22 ± 0.01	15.50 ± 0.03	1	12.75 ± 0.03	12.66 ± 0.03	12.66 ± 0.06	12.71 ± 0.07	...	0	CIII
4.....	08065158-4728058	14.55 ± 0.01	13.34 ± 0.01	12.03 ± 0.01	1	10.20 ± 0.03	10.25 ± 0.03	10.21 ± 0.03	10.19 ± 0.03	...	0	CIII
5.....	08065419-4730210	14.54 ± 0.01	13.34 ± 0.01	12.05 ± 0.01	1	10.23 ± 0.03	10.25 ± 0.03	10.20 ± 0.03	10.17 ± 0.03	...	0	CIII
6.....	08070052-4732093	13.58 ± 0.01	12.82 ± 0.01	12.03 ± 0.01	1	10.98 ± 0.03	11.01 ± 0.03	10.99 ± 0.03	11.00 ± 0.03	...	0	CIII
7.....	08070716-4721462	12.99 ± 0.01	11.90 ± 0.01	10.74 ± 0.01	1	9.16 ± 0.03	9.18 ± 0.03	9.16 ± 0.03	9.12 ± 0.03	1.59 ± 0.61	0	CIII
8.....	08071155-4719512	16.09 ± 0.01	14.77 ± 0.01	13.13 ± 0.01	1	11.10 ± 0.03	11.10 ± 0.03	11.07 ± 0.03	11.05 ± 0.03	...	0	CIII
9.....	08071312-4721124	18.05 ± 0.01	16.60 ± 0.01	14.03 ± 0.01	1	11.35 ± 0.03	11.33 ± 0.03	11.26 ± 0.03	11.22 ± 0.03	...	0	CIII
10.....	08071363-4725155	13.39 ± 0.01	12.73 ± 0.01	11.94 ± 0.01	1	10.86 ± 0.03	10.84 ± 0.03	10.81 ± 0.03	10.83 ± 0.03	...	0	CIII

NOTES.—Table 1 is published in its entirety in the electronic edition of the *Astrophysical Journal*, including 2MASS photometry. A portion is shown here for guidance regarding its form and content.

REFERENCES.—(1) This work; (2) Kharchenko 2001.

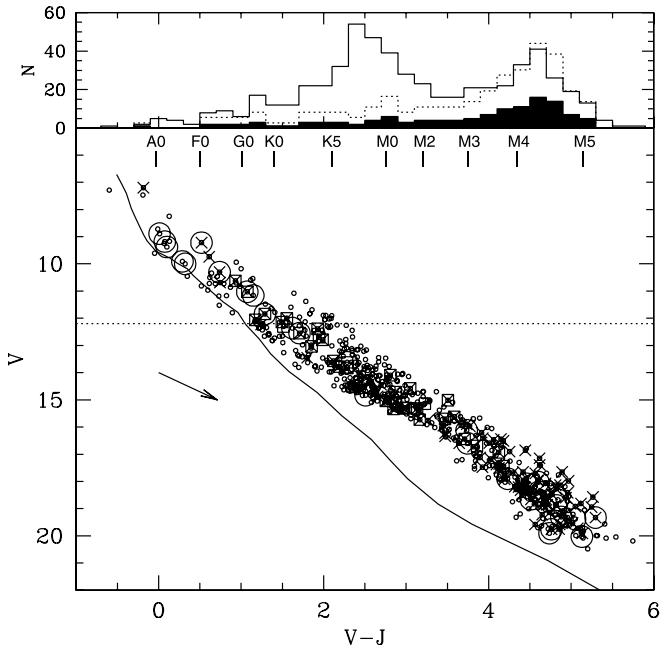

FIG. 3.—Color magnitude diagram illustrating the contamination level of the photometric candidates sample. The top panel shows the $V-J$ distributions for the high-probability member sample (*solid histogram*) and the photometric candidates (*open histogram*). Using the stars with $V-J>3.5$ (where the contamination level is low), we normalized both distributions to estimate the expected members distribution (*dashed histogram*). It is apparent that the number of photometric candidates increases in the color range $1.5<V-J<3.5$, where the giant branch crosses our sample. In this range, the contamination level by nonmembers is quite high (∼68%). In the bottom panel symbols are similar to those in Fig. 2. We plotted the location of the spectral type sequence, using the standard $V-J$ color from Kenyon & Hartmann (1995). Stars with infrared excess detected in § 4 are represented as open circles. The dotted line represents the completeness limit for MIPS photometry assuming $K-[24]\sim 0$ (photospheric color) and the 5 Myr isochrone (Siess et al. 2000) at 350 pc with a reddening of $A_V=0.2$ (spectral type ∼ K3). [*See the electronic edition of the Journal for a color version of this figure.*]

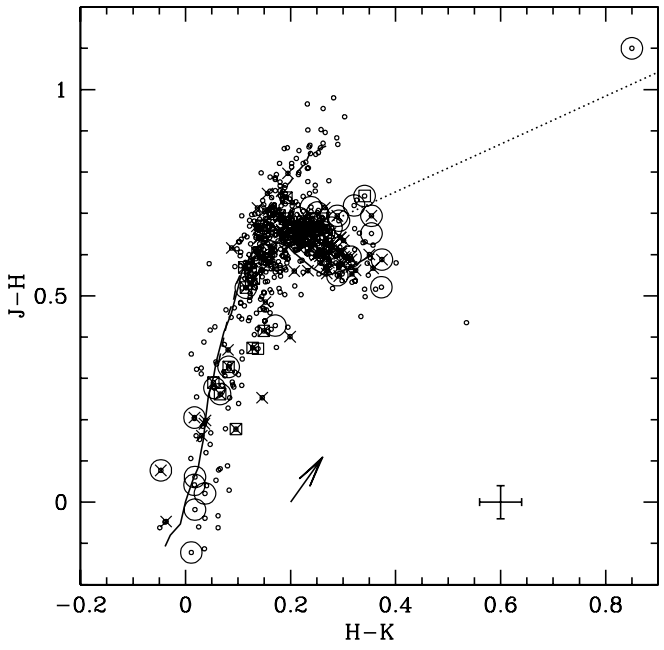

FIG. 4.—2MASS color-color diagram, $J-H$ versus $H-K$, illustrating the selection of M giant stars in the field of view of the γ Velorum cluster. Solid and dashed lines represent the standard sequence from Bessell & Brett (1988) for dwarfs and giants, respectively. The arrow indicates the reddening vector for $A_V=1$. The error bar represents the typical 2MASS color uncertities in our sample. As a reference, we plot the loci of classical T Tauri stars (CTTSs) defined by Meyer et al. (1997). Other symbols are the same as Fig. 3. [*See the electronic edition of the Journal for a color version of this figure.*]

giants in this diagram. We have selected 27 stars in the locus of giants with $J-H\geq 0.8$; these stars are labeled in Table 1 as M-type giant candidates. Taking into account this M giant sample, the contamination level where the giants branch crosses the γ Velorum sequence in Figure 3 is still high (≳66%).

4. DISK DIAGNOSTICS

Figure 5 shows three diagrams used to identify and characterize stars bearing disks in the γ Velorum cluster. The top panel shows the SED slope, determined from the $[3.6]-[8.0]$ color (SED slope $=d\log[\lambda F_\lambda]/d\log[\lambda]$) versus the [8.0] magnitude. Dotted lines represent the 3 σ boundaries (photospheric level), which is calculated using the photometric errors propagated from the $[3.6]-[8.0]$ color (Hernández et al. 2007a, 2007b). Stars with excess emission at 8 μm can be identified in this diagram above the photospheric limit. In general, disk-bearing stars in Taurus (Hartmann et al. 2005) are located above the dotted line, with an IRAC SED slope >-1.8 (see Lada et al. 2006; Hernández et al. 2007b); this limit is used to identify objects with optically thick primordial disks (Class II). Half of the stars with IRAC excesses are located below the Class II region suggesting that the disks around these stars have evolved significantly and are in an intermediate phase between stars with optically thick disks and debris disk stars. We call these evolved disks.

The bottom left panel shows the $V-J$ versus $K-[24]$ color-color diagram, in which we identify stars with 24 μm infrared emission above the photospheric level (e.g., Gorlova et al. 2004, 2006; Hernández et al. 2006, 2007a). The $K-[24]$ color distribution of stars with $K-[24]<1.0$ describes a Gaussian centered at $K-[24]=0.05$ with $\sigma=0.14$. The 3 σ boundaries (*dotted lines*) represent the photospheric region at 24 μm; stars with 24 μm excesses are located redward from this region. Except for the three faintest stars with excesses at 8 μm (*inverse triangles in the top panel*), all stars with IRAC excess have excess at 24 μm. Our sample of disk-bearing candidates includes 14 stars with excess at 8 and 24 μm, 3 stars with excess at 8 μm and with no MIPS detection, and 12 stars with excess at 24 μm and photospheric color in the IRAC bands.

Using the standard $V-J$ colors in Figure 3 (or in the bottom left panel of Fig. 5), we can estimate the spectral types of stars with infrared excesses. We use three bins: early-type stars ($V-J\leq 0.54$; F0 or earlier); solar-type stars ($0.54<V-J<2.0$; from early F to early K); and late-type stars ($V-J>2.0$; K5 or later). The bottom right panel of Figure 5 displays the distribution of the disk-bearing stars in a SED slope diagram, generated using the $K-[5.8]$ and $[8.0]-[24]$ colors. The $[8.0]-[24]$ SED slope indicates whether the star has a flat or a rising SED (SED slope ≥ 0) at wavelengths greater than 8.0 μm and hence whether it should be classified as a flat-spectrum or a Class I source.

We can also compare the properties of disks in the γ Velorum cluster to those disks with strong evidence of dust evolution. Primordial disks with a high degree of inner disk clearing have been called transitional disks; observationally they are characterized by relatively small excess below 5.8 μm and a large excess at longer wavelengths, implying an SED slope $[8.0]-[24]>0$ (Hernández et al. 2007b). We show in Figure 4 the location of four well-known transitional disks in Taurus, Chameleon, and the TW Hya association: TW Hyd (4), GM Aur (5), Coku Tau (6), and CS Cha (7) (Calvet et al. 2002, 2005; D'Alessio et al. 2005b;

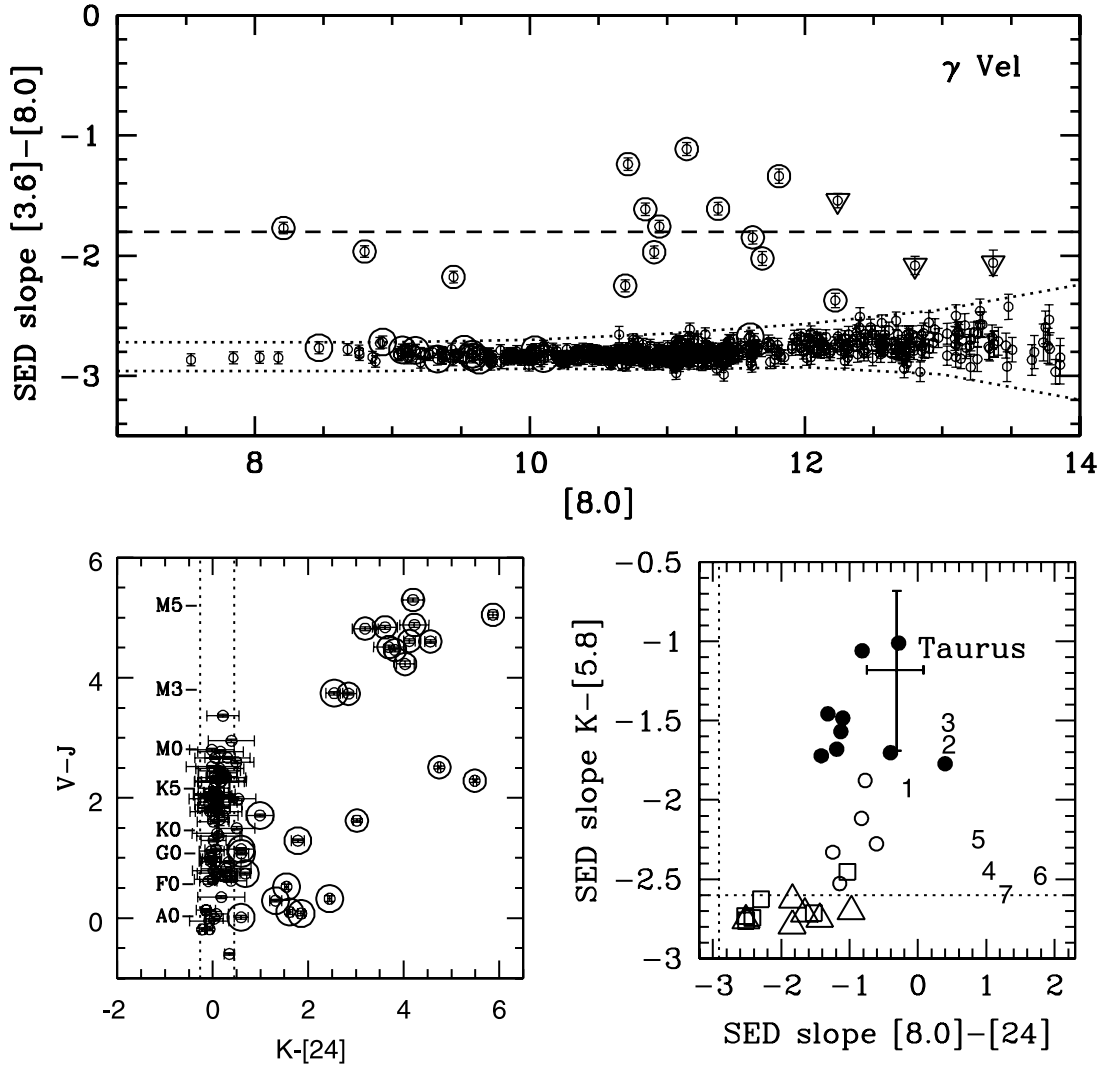

FIG. 5.—Diagrams illustrating the detection of disks based on their infrared emission above the photospheric levels (*dotted lines*). The top panel shows the IRAC SED slope diagram indicating stars with excess at 8 μm. The dashed line represents the Class II limit proposed by Lada et al. (2006), and the inverse triangles are objects with IRAC excess but lacking MIPS detections. Stars with 24 μm excess are represented by points surrounded by large open circles. The color magnitude diagram $V - J$ vs. $K - [24]$ is displayed in the bottom left panel illustrating the detection of stars with excess at 24 μm. The bottom right panel shows the SED slope for $K - [5.8]$ versus the SED slope for $[8.0] - [24]$ diagram. Disk-bearing stars in different spectral type ranges are plotted with different symbols, stars with spectral type A are represented with open triangles, stars from F to early-K with open squares and late-type stars (K5 and later) with circles. The error bar represents the median and quartiles for the Taurus disks (Hartmann et al. 2005; Furlan et al. 2006); solid circles are stars with disk emission similar than Taurus's disk population (Class II objects). As reference, we also mark the locations of stars in other star-forming regions believed to have pretransitional (1, 2, and 3; Espaillat et al. 2007a; Furlan et al. 2006) and transitional disks (4, 5, 6, and 7; Calvet et al. 2002, 2005; D'Alessio et al. 2005b; Espaillat et al. 2007b). One Class II object is a pretransitional disk candidate. [*See the electronic edition of the Journal for a color version of this figure.*]

Espaillat et al. 2007b). In addition, we show in Figure 4 the location of the newly discovered class of pretransitional disks, in which gaps in primordial disks rather than holes have been identified (Espaillat et al. 2007a; Brown et al. 2008). These are LkCa 15 (1), UX Tau (2), and HK Tau (3) (Espaillat et al. 2007a; Furlan et al. 2006). In contrast to the disk population in the σ Orionis cluster, the Orion OB1b association, and the 25 Orionis aggregate (with ages of $\sim$3, 5, and 8 Myr, respectively, Hernández et al. 2007a, 2007b), there are no transitional disk candidate detected in the γ Velorum cluster. However, there is a pretransitional disk candidate (star 52; labeled as PTD in Table 1) with infrared excesses similar to the pretransitional disk systems UX Tau and Lk Ca 15 (Espaillat et al. 2007a).

The late-type stars exhibit less infrared excess than the disk population in Taurus, suggesting that the disks in the γ Velorum cluster have evolved substantially.

Except for one solar-type star (see § 4.2), which exhibits IRAC and MIPS excesses, the early-type and solar-type stars show excesses only at 24 μm. The relatively small 24 μm excess ($K - [24] < 3$) of these objects are consistent with their being debris disks, in which second generation dust is produced by collisions between planetesimals (e.g., Kenyon & Bromley 2005; Hernández et al. 2006; Currie et al. 2008). However, theoretical models of collisional cascade at 30–150 AU Kenyon & Bromley (2005) do not predict enough excess emission to explain the observed excesses at 5 Myr. A small dust contribution from collisional cascade in the inner disk (<30 AU) or remaining primordial dust in the disk could explain these differences (see Hernández et al. 2006). Since the timescale for primordial disk dissipation decreases as the stellar mass increases (e.g., Hernández et al. 2007a; Lada et al. 2006), observations of remaining primordial dust are more likely in the disk around solar-type stars than in early-type stars.

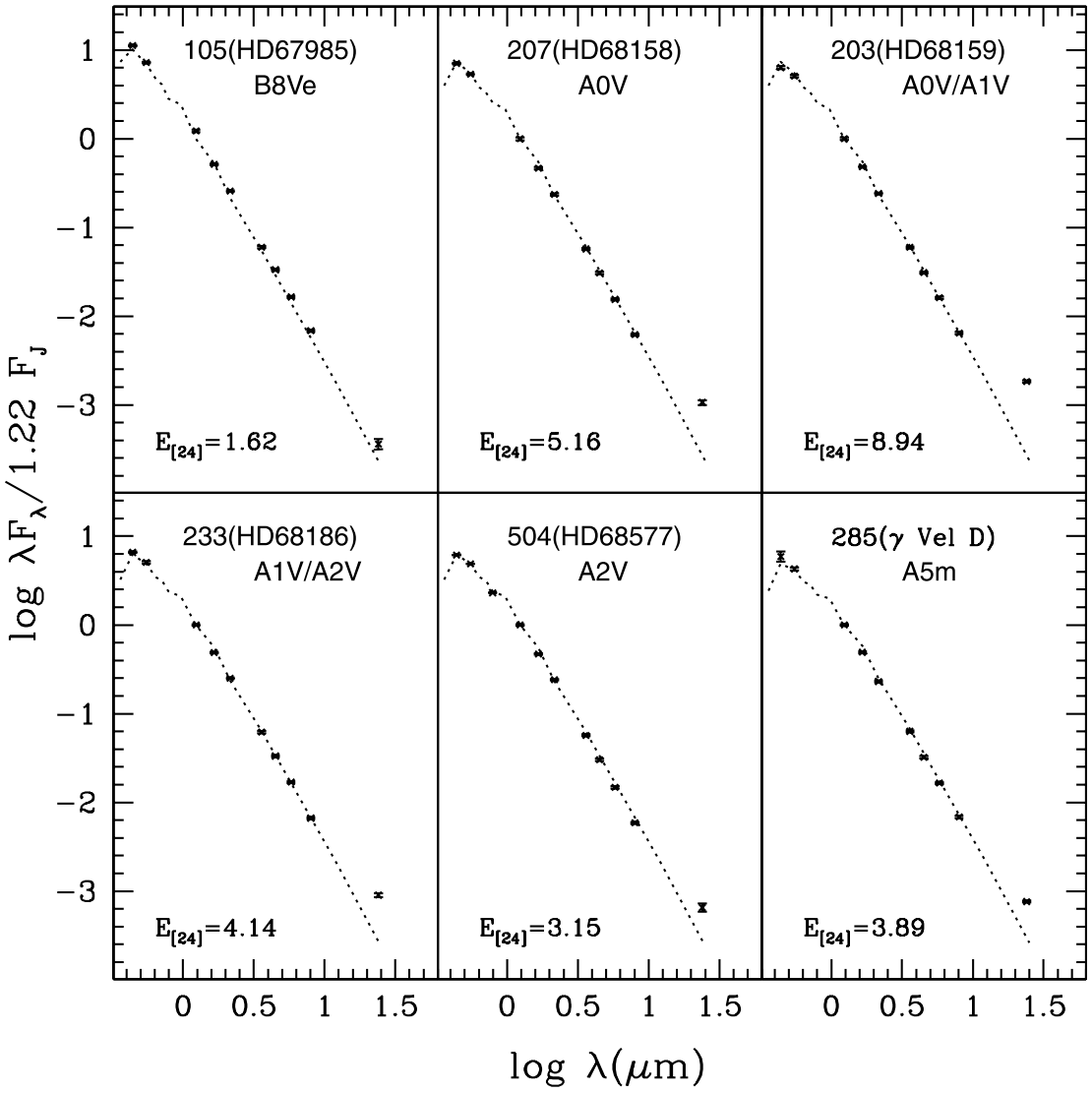

FIG. 6.—SEDs for A-type stars with infrared excess. Each panel shows the spectral type of the object (Houk 1978; Abt et al. 1976), and the excess ratio, E_{24} (Rieke et al. 2005), calculated from the $K - [24]$ color. Dotted lines show the corresponding photospheric colors (Kenyon & Hartmann 1995). Star 105 (*top left panel*) is a Be star, the other five stars are debris disk candidates.

Visual inspection of the IRAC and MIPS images reveals that stars with infrared excesses are not contaminated by artifacts, nebulosity, or extragalactic sources. In general, the stars with infrared excesses are isolated sources. Only stars 115 and 359 have nearby faint sources (within the background photometric annulus) that could affect the photometry at [3.6] and [4.5]; however, these objects look like isolated objects at longer wavelengths, where infrared excesses are more obvious. The star 8797 (with elongated PSF) can be a close binary not resolved by IRAC. For this source, IRAC and MIPS photometry includes contributions from both components.

4.1. *Disks of Early-Type Stars*

We detected six early-type stars with excess at 24 μm. Figure 6 shows the SEDs of these objects. Except for the star 285 (γ Vel D; Abt et al. 1976), a binary star near the γ Velorum system, all stars have spectral types from Houk (1978).[10] Abt et al. (1976) classified γ Vel D as a metallic-lined binary star with spectral type ranging from A2 to A8; we assumed a spectral type of A5 in Figure 6.

Color excesses (E_{V-J}) were obtained by interpolating spectral types in the table of standard $V - J$ color given by Kenyon & Hartmann (1995). SEDs were corrected for reddening (A_V) using E_{V-J} and the extinction relation from Cardelli et al. (1989) with the value of total to selective extinction for normal interstellar reddening ($R_V = 3.1$). The small values of A_V obtained (average $= 0.2 \pm 0.1$) support the low reddening reported for the γ Velorum cluster (Abt et al. 1976; Pozzo et al. 2000; R. D. Jeffries et al. 2008, in preparation). We use the color $K - [24]$ to determine the excess ratio at 24 μm (e.g., Rieke et al. 2005), $E_{24} = 10^{(K-[24]-0.05)/2.5}$, where 0.05 is the mean value of $K - [24]$ for the photometric candidates with MIPS detections.

Star 105 exhibits a very small excess at 24 μm. As it is also an emission-line star (Houk 1978; MacConnell 1981) and its 2MASS colors are similar than those observed in classical Be stars (Hernández et al. 2005), this excess is likely to be free-free emission in a hot envelope—that is, this is probably the excess of a classical Be star. The remaining stars with 24 μm excesses are likely to be debris disk systems with E_{24} similar to those observed in

[10] Vizier Online Data Catalog III/51B (N. Houk 1978).

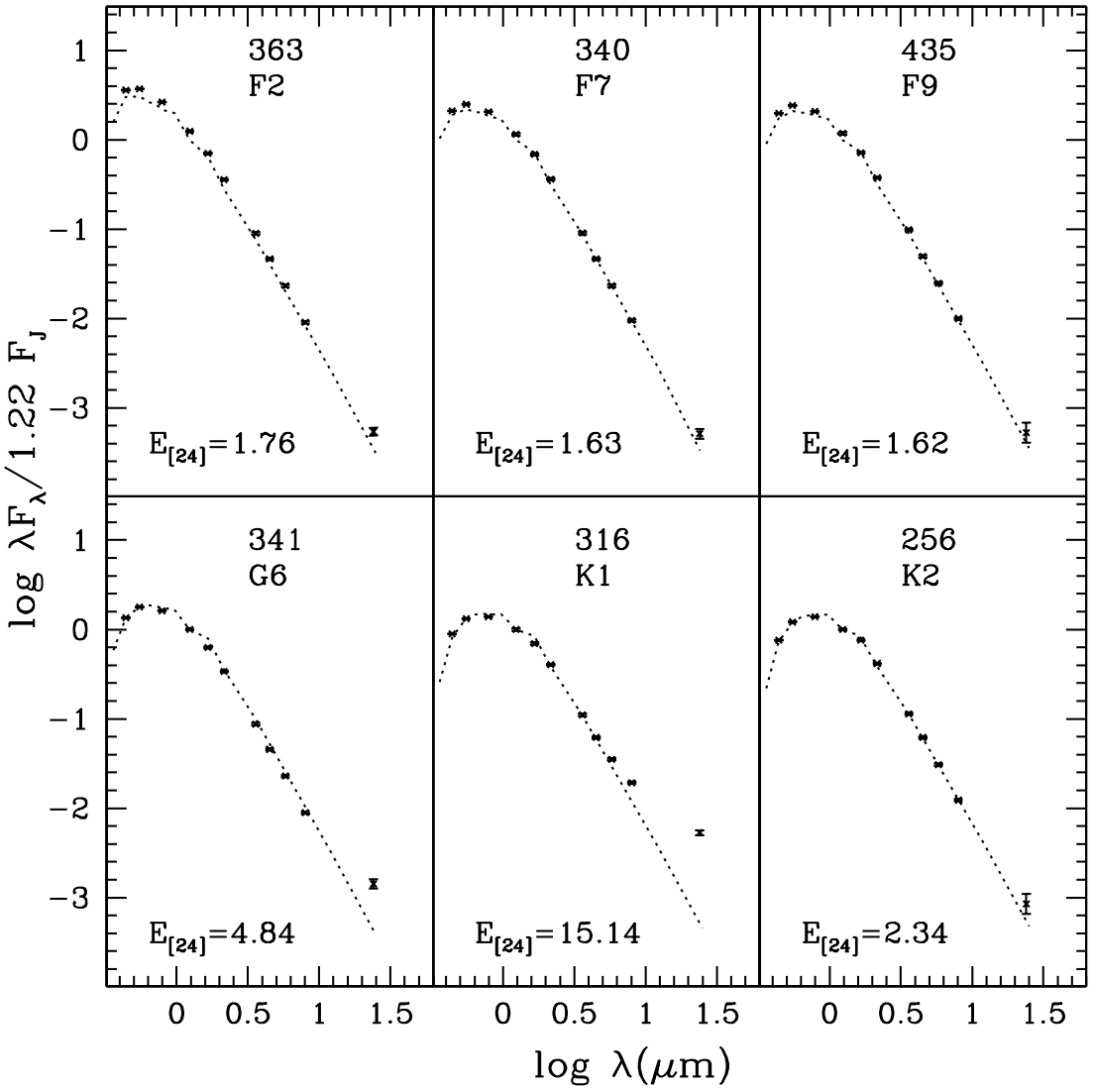

FIG. 7.—SEDs for solar-type stars with infrared excesses. Each panel shows the photospheric spectral type calculated from the color $V - J$ assuming a reddening of $A_V = 0.15$ mag and intrinsic colors from Kenyon & Hartmann (1995). Dotted lines represent the corresponding photospheric level (Kenyon & Hartmann 1995). The excess ratio at 24 μm is displayed in each panel.

debris disks candidates of the σ Orionis cluster and the Orion OB1b subassociation (Hernández et al. 2006, 2007a).

Most of stars with $V - J \leq 0.54$ (F0 or earlier) have spectral types from Houk (1978) or Kharchenko (2001). Except for the stars 277 and 572, the published spectral type and the photometric spectral type calculated from the $V - J$ color (see Fig. 3) agree within five spectral subclasses. However, additional studies (e.g., radial velocity) are necessary to confirm membership of our early-type sample. Assuming that stars 277 and 572 are not members of the γ Velorum cluster, we find eight early-type candidates without infrared excess (diskless), five debris disk candidates, and one classical Be star. Since some diskless candidates could not be members of the cluster, the debris disk frequency estimated in this work (5 debris disks/14 early-type stars; $\sim$36% $\pm$ 16%) is a lower limit.

Adams et al. (2004) report that mechanisms of gas dispersal, like photoevaporation, can disrupt planet formation in two important ways: (1) if the gas is dispersed before the disk dust has grown to centimeter size, the formation of planetesimals will be curtailed as the dust is removed with the gas; (2) if the gas is dispersed before large rocky planets are formed, the formation of gas giant planets like Jupiter will be suppressed. The debris disk frequency ($\gtrsim$36%) and the infrared emission from the debris disks in the γ Velorum cluster are comparable to the debris disk population of stellar groups with similar ages. For instance, using the same method to detect stars with excess at 24 μm, Hernández et al. (2006) reported debris disk frequency of $\sim$38% $\pm$ 3% and $\sim$46% $\pm$ 4% for the Orion OB1b subassociation ($\sim$5 Myr) and for the 25 Orionis stellar aggregate ($\sim$8 Myr), respectively. Since the presence of debris disks implies the formation of kilometer size objects (Kenyon & Bromley 2005), proposal 1 appears unlikely.

4.2. *Disks around Solar-Type Stars*

We detected six solar-type stars with excesses at 24 μm. Figure 7 shows the SEDs for this subsample. Each panel shows the corresponding photospheric fluxes (Kenyon & Hartmann 1995). Spectral types were estimated by interpolating dereddened $V - J$ colors using the standard table given by Kenyon & Hartmann (1995). We assumed a reddening value of $A_V = 0.15$ ($E_{V-I} = 0.06$; Pozzo et al. 2000).

The values of E_{24} in this subsample are slightly smaller than the debris disks around FGK stars observed in the 15 Myr old

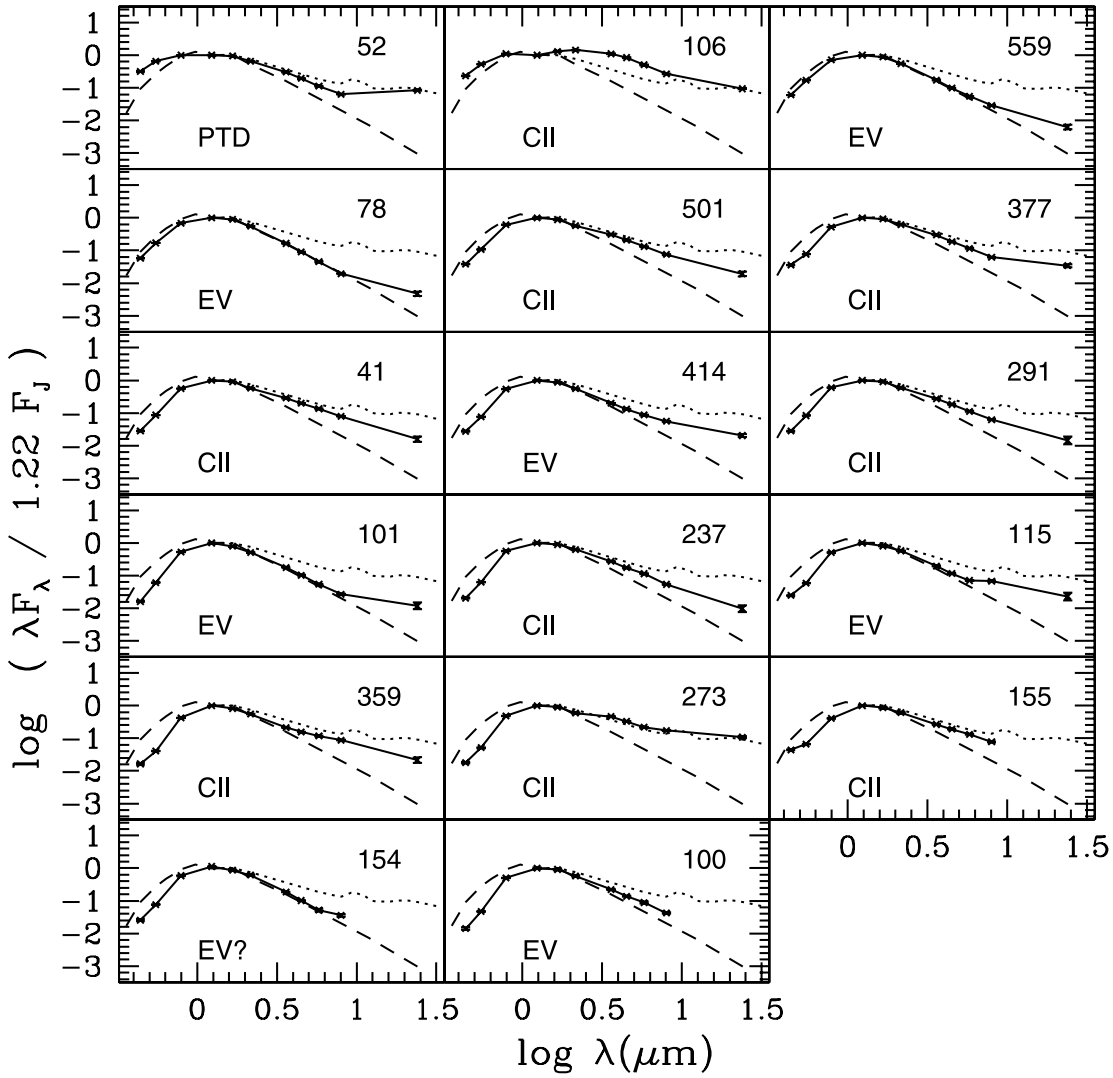

FIG. 8.—SED for low-mass stars with infrared excess (*solid lines*). Dotted and dashed lines represent the median SED for Class II stars in Taurus (Furlan et al. 2006), and the photospheric fluxes for stars with spectral type M2 (Kenyon & Hartmann 1995), respectively. Each panel shows the disk classification: pretransitional disks (PTD), Class II objects (CII), and evolved disk objects (EV).

Scorpius-Centaurus-Lupus subassociation (Chen et al. 2005; Siegler et al. 2007) and comparable to the excesses of debris disks around FGK stars in the 30 Myr old cluster NGC 2547 (Gorlova et al. 2007). Assuming the same excess detection threshold of $E_{24} = 1.41$ ($K - [24] = 0.42$), we have calculated a median E_{24} of $2.1^{+4.8}_{-1.6}$, $2.8^{+14.2}_{-2.0}$, and $2.0^{+2.3}_{-1.5}$ for FGK-type debris disk candidates in the γ Velorum cluster, Scorpius-Centaurus-Lupus subassociation and the NGC 2547 cluster, respectively. The errors represent the upper and lower quartiles of each sample. If interpreted as an evolutionary sequence, these disk emissions would be consistent with a growth period of dust production and a following decrease as dust particles are removed, as predicted by theory (Kenyon & Bromley 2005). Similar trends have been seen in A-type stars (Hernández et al. 2006; Currie et al. 2008). However, given the small number of stars, the statistical significance of this result is low.

Only star 316 shows an excess at shorter wavelengths; it represents the earliest star exhibiting excess in the IRAC bands. The excesses around this star can be explained if the disk is in an intermediate phase evolving from a primordial to a debris disk (evolved disk). Another possibility is that this star has a very massive debris disk produced recently by a catastrophic collision between two planetary-size bodies (Gorlova et al. 2007; Kenyon & Bromley 2005).

4.3. *Disks around Late-Type Stars*

Figure 8 shows the SEDs of late-type stars sorted by brightness in the V band. We display the median SED of optically thick disk stars in Taurus (Furlan et al. 2006) and the photospheric fluxes for a star with spectral type M2 (Kenyon & Hartmann 1995). The diversity of disks in the γ Velorum cluster is apparent. We distinguish between Class II systems (CII, with SED slopes $K - [5.8] > 1.8$) and evolved disk (EV) systems exhibiting smaller IRAC/MIPS excesses than Class II systems ($K - [5.8] < 1.8$).

Two stars have photometric colors between K5 and M0; one of them (star 52) shows infrared excesses similar to pretransitional disks objects (Espaillat et al. 2007a). The other star (106) exhibits larger infrared excesses than the optically thick median in Taurus. The next two objects (stars 559 and 78), with photometric spectral type ~M3, exhibit modest infrared emission, which could be explained by decreasing the height of the irradiation surface in the disks due to a higher degree of settling producing flatter disk structures (Hernández et al. 2007a, 2007b; D'Alessio et al. 2006). The remaining 13 stars with infrared excesses have

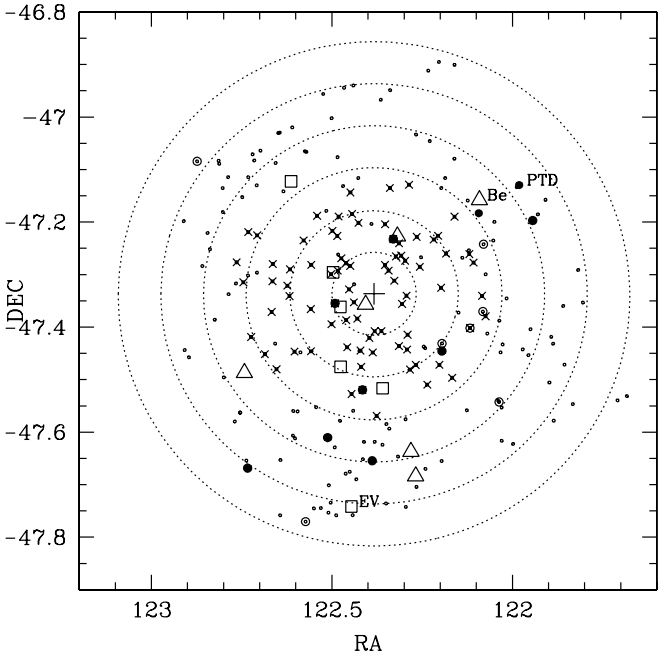

FIG. 9.—Space distribution of stars with infrared excesses. Symbols for stars with infrared excess are the same as the bottom right panel of Fig. 5. We display X-ray sources (*crosses*) and photometric candidates (*small open circles*) with $V - J > 3.5$ (little contamination is expected in this color range) Dotted circles represent projected distance from the γ Velorum system in intervals of 0.5 pc. We mark the position of the solar-type star with IRAC excess (EV), the Be star (Be), and the pretransitional disk candidate (PTD). [*See the electronic edition of the Journal for a color version of this figure.*]

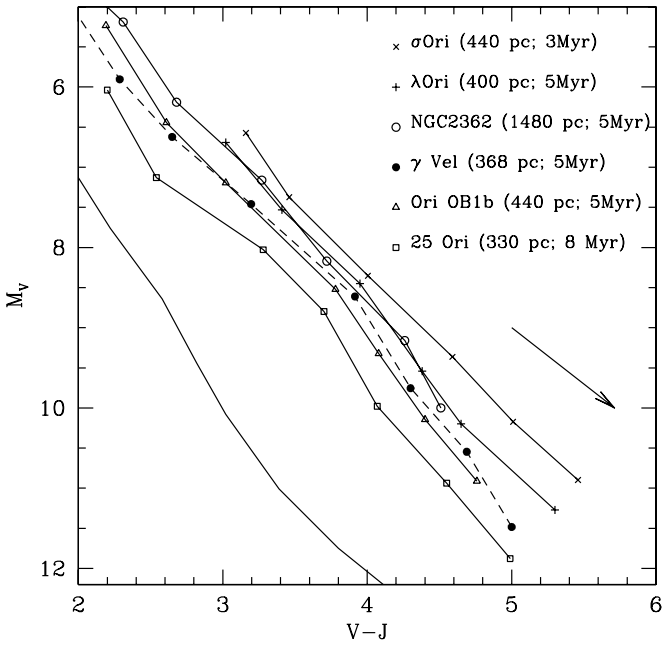

FIG. 10.—Color–absolute magnitude diagram comparing the median color and magnitudes of members of several 5 Myr old stellar populations and the γ Velorum cluster. As reference, the ~8 Myr old cluster 25 Orionis and the ~3 Myr old cluster σ Orionis are also displayed. The arrow indicates the reddening vector for $A_V = 1$. It is apparent that the γ Velorum cluster has similar colors to the other 5 Myr old stellar groups. [*See the electronic edition of the Journal for a color version of this figure.*]

photometric spectral types M4 or later (see Fig. 3) suggesting, as in other young stellar population (Hernández et al. 2007a, 2007b; Carpenter et al. 2006; Lada et al. 2006), that primordial disk frequencies depend on the mass of the central object. Using the number of members expected in our photometric sample (Fig. 3, *dashed histogram*), we calculated disk fractions of $4.3\% \pm 3.0\%$ for the color range $2 < V - J < 3$ (~K5–M1), $3.5\% \pm 2.4\%$ for the color range $3 < V - J < 4$ (~M1–M3.5), and $7.1\% \pm 2.0\%$ for stars in with $V - J > 4$ (later than M3.5).

Stars 100, 154, and 155 are too faint to be detected by MIPS. Two of them show excesses in all IRAC bands, making identification of these stars (100 and 155) as having dust disks fairly certain. However, star 154 shows excess only at 8 μm, which could be produced by either disk emission or PAH contamination.

Figure 9 shows the spatial distribution of the stars with infrared excesses in our sample. Different spectral type ranges are represented with different symbols. As reference, we identify X-ray sources and photometric candidates with $V - J > 3.5$ (little contamination by nonmembers is expected in this color range). The projected distances from the γ Velorum system are displayed in intervals of 0.5 pc. One debris disk is located inside 0.25 pc, while the only optically thick disks are in systems located at projected distances of $\gtrsim$0.5 pc. Since, about 10% of the stars bearing disks are expected to have transitional disks (Hernández et al. 2007b; J. Muzerolle J. 2008, in preparation), we can expect one or two transitional disks in the γ Velorum cluster. However, we did not detect any transitional disk objects in the cluster. We can speculate that external mechanisms of disk dispersal (like photodissociation and/or photoionization by strong stellar winds and/or strong UV radiation), affecting mainly the disk surface and the outer region of the disk, combined with the fast inner clearing characterizing transitional disks, decrease the probability of observing a disk in this phase. Given the small number of stars bearing disks, the statistical significance of this speculation is very low.

5. COMPARISON WITH OTHER YOUNG STELLAR POPULATIONS

To compare the disk frequencies in γ Vel with other regions, we need to estimate the cluster age, which depends to some extent on the assumed distance to the cluster. Burningham (2005) confirmed that this group is a stellar cluster belonging to the Vela OB2 association, analogous to the σ Orionis cluster in the Orion OB1b subassociation (Hernández et al. 2007a). The primary star in the γ Vel system is the only WR star with a distance from *Hipparcos* (258^{+41}_{-31} pc; Schaerer et al. 1997); but this distance is in marked contrast to distances estimated by other methods (350–450 pc) and to the *Hipparcos* distance of the Vela OB2 association (410 ± 12 pc; de Zeeuw et al. 1999). Using interferometric observations to estimate the geometrical parameters of the orbit of the γ Vel system, Millour et al. (2007) and North et al. (2007) give distances of 368^{+38}_{-13} and 336^{+8}_{-7} pc, respectively. These values are in agreement with the distance obtained by van Leeuwen (2007; 349^{+44}_{-35} pc) with the new reduction of the *Hipparcos* data that includes modeling of the satellite dynamics and eliminates the data correlation in the original catalog caused by attitude-modeling errors (Maíz Apellániz et al. 2008). The age estimated by North et al. (2007; 3.5 Myr) for the O star is in agreement with the age estimated by Pozzo et al. (2000; $\lesssim$5 Myr) for the cluster and the age estimated by De Marco & Schmutz (1999; 3.6 Myr) for the γ Vel system. We assume the corrected *Hipparcos* distance of 350 pc, which is in agreement within 1.5 σ from the distance calculated by Millour et al. (2007) and North et al. (2007) and a reference age of 5 Myr.

To support the assumed age, we plot in Figure 10 the median absolute magnitudes versus the median $V - J$ color for members of several different stellar groups. Regardless of the uncertainties

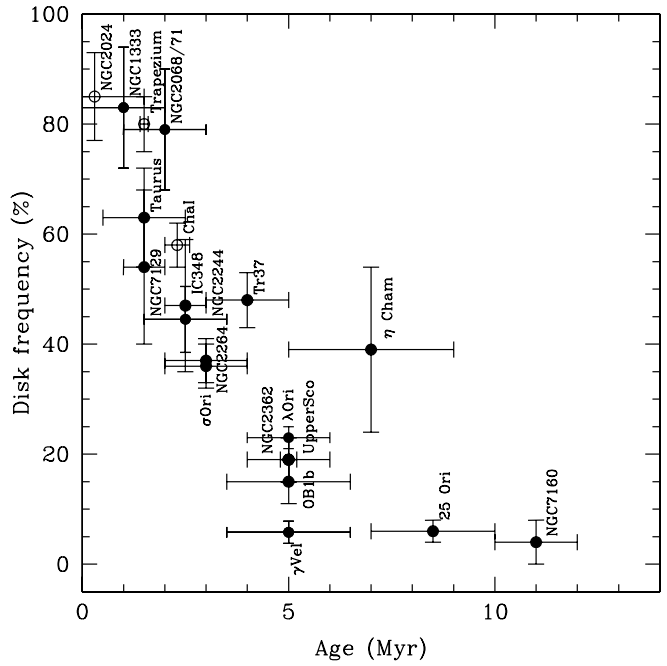

FIG. 11.—Fraction of stars with near-infrared disk emission as a function of the age of the stellar group. Open circles represent the disk frequency for stars in the T Tauri (TTS) mass range (∼K5 or later), derived using *JHKL* observations: NGC 2024 and Trapezium (Haisch et al. 2001), and Chameleon I (Gómez & Kenyon 2001). Solid symbols represent the disk frequency calculated for stars in the TTS mass range using *Spitzer* data (see text for references).

introduced by theoretical evolutionary tracks, Figure 10 shows that the γ Velorum cluster is in a similar evolutionary stage as the other stellar groups with ages normally quoted as ∼5 Myr: the λ Orionis cluster (Barrado y Navascués et al. 2007; Dolan & Mathieu 2002), the cluster NGC 2362 (Dahm & Hillenbrand 2007), and the Orion OB1b subassociation (Briceño et al. 2007; Hernández et al. 2007b). We estimate an error of 1.5 Myr comparing the standard deviation in the color $V-J$ for the member sample (see § 3) to the standard deviation obtained using the theoretical isochrones from Siess et al. (2000) with a reference age of 5 Myr.

Figure 11 shows the disk frequencies of late-type stars (stars K middle or later) with near-infrared disk emission in different stellar groups, as a function of age (Hernández et al. 2005, 2007a; Haisch et al. 2001). Using the number of members with $V-J>2.0$ (∼K5 or later) expected in our photometric sample (Fig. 3, *dashed histogram*) and the disk detected in § 4.3, we calculated a primordial disk frequency of 6% ± 2% for the γ Velorum cluster. We include recent *Spitzer* results for the young stellar clusters NGC 1333 (Gutermuth et al. 2008), NGC 2068/71 (Flaherty & Muzerolle 2008), Taurus (Hartmann et al. 2005), NGC 7129 (Gutermuth et al. 2004), Chameleons (Megeath et al. 2005), Tr 37 and NGC 7160 (Sicilia-Aguilar et al. 2006), IC 348 (Lada et al. 2006), NGC 2244 (Balog et al. 2007), NGC 2264 (Cieza & Baliber 2007), σ Ori (Hernández et al. 2007a), NGC 2362 (Dahm & Hillenbrand 2007), λ Ori (Barrado y Navascués et al. 2007), Upper Scorpius (Carpenter et al. 2006), and Orion OB1b and 25 Ori (Hernández et al. 2007b).

The disk frequencies decrease toward older ages with a timescale for primordial disk dissipation of ∼5 Myr. It is apparent that the disk frequency found in the γ Velorum cluster is lower than that found in young stellar populations with similar ages, and comparable to the disk frequency in older stellar groups. This could indicate that the low disk presence observed in the γ Velorum cluster is abnormal for its evolutionary stage, and environmental effects, such as strong stellar winds and/or strong radiation fields from the γ Velorum system, could provide the physical mechanism for the low disk frequency. Moreover, ∼75% of the disk-bearing stars in the γ Velorum cluster show IRAC SED slopes smaller than the median values of other 5 Myr old stellar groups plotted in Figure 10 suggesting that the disks of the γ Velorum cluster have a higher degree of dust settling. In particular, the median IRAC SED slopes for the disk population of NGC 2362, the λ Orionis cluster, the OB1b subassociation and the γ Velorum cluster are −1.72, −1.60, −1.70, and −1.82, respectively (with a typical error of 0.06).

Studying the young (2–3 Myr) open cluster NGC 2244, Balog et al. (2007) showed that high-mass stars (O-type stars) can affect the primordial disks of lower mass members only if they are within ∼0.5 pc of the high-mass star. We find similar results for the γ Velorum cluster. Using the photometric members with $V-J>3.5$ (∼M2 or later), we find a disk frequency of 4% ± 3% at a projected distance of 0.25–1.0 pc; inside 0.25 pc the central objects of the cluster contaminate the optical photometry used to select photometric candidates (§ 3). The closest primordial disk is located at projected distance of ∼0.5 pc. At larger projected distance (>1.0 pc), the disk frequency is larger (8% ± 2%). This suggests that the relative fast dispersion of disks in the γ Velorum cluster is produced by the strong radiation fields and strong stellar winds from the central objects. This result must still be considered tentative given the small number of stars with disks, which results in large errors in disk frequencies.

Alternatively, Figure 11 indicates that the disk frequency drops rapidly at ∼5 Myr and the relative low frequency of disks observed in the γ Velorum cluster could be explained if the cluster is slightly older than 5 Myr. Additional studies of photometric members presented in Table 1 are necessary to explain the disk population found in γ Velorum cluster.

6. CONCLUSIONS

We have used the IRAC and MIPS instruments on board the *Spitzer Space Telescope* to conduct a study of disks around the γ Velorum cluster. Since the central object is a binary system consisting of the closest known Wolf-Rayet star and a high-mass O star, a strong UV radiation field and stellar winds are present in the cluster. Using optical photometry of X-ray sources (2XMM) and members confirmed by spectroscopy (R. D. Jeffries et al. 2008, in preparation), 579 photometric candidates were selected as possible members of the cluster. The level of contamination by nonmembers depends on the $V-J$ color range, showing the highest level of contamination (∼68%) at $V-J=1.5$–3.5, where the field giant branch crosses the young stellar population. Combining optical, 2MASS, and *Spitzer* data we have detected infrared excess in 29 stars. One of the infrared excess stars is a Be star. We report five debris disks around A-type stars, five debris disks around solar-type stars (spectral type range F to early K) and one solar-type star with infrared excess produced by a very massive debris disks or by a primordial disk with a high degree of dust settling. Seventeen disk-bearing low-mass stars (K5 or later) were found in the cluster with a range of disk properties. We classified these objects in three classes using the infrared excess at 5.8 μm and the SED slope $[8.0]-[24]$: nine Class II stars, seven evolved disks star, and one pretransitional candidate. We found that 76% of the stars bearing primordial disks have color $V-J>4$ (∼later than M3.5), indicating a mass-dependent timescale for disk dissipation in the γ Velorum cluster, similar

to results in other young star populations (Carpenter et al. 2006; Hernández et al. 2007a, 2007b; Lada et al. 2006).

We found that the disk frequency observed in the γ Velorum cluster is lower than in other young stellar groups with similar ages ($\sim$5 Myr), and comparable to values found in older populations ($\sim$10 Myr). Empirical isochrones support the age of $\sim$5 Myr for the overall population of the γ Velorum cluster. The relative low frequency observed in the cluster is consistent with: (1) rapid disk dissipation due to the influence of the strong radiation fields and winds from the WR and O star cluster members or (2) the age of the cluster is slightly older and the low frequency reflects the fast dropping in disk frequency observed at $\sim$5 Myr. More than 75% of the primordial disk stars have inner disk emission lower than the median observed in the disk population of other 5 Myr clusters, indicating that the disks of the γ Velorum cluster have a larger degree of dust settling.

We find no primordial disks closer than $\sim$0.75 pc from the high-mass central binary. At projected distance >1 pc, the disk fraction seems to be constant around 5%–7%. This result is similar to that found in the NGC 2244 cluster (Balog et al. 2007) in which primordial disks are affected only in the immediate vicinity of the O stars ($<$0.5 pc). Our results reinforce an emerging trend in studies of disk frequency, specifically that optically thick disk dissipation is rapid for $\sim$90% of systems, lasting less than 5 Myr, while $\sim$10% of disks can last for 8 Myr or more.

We thank Aletta Tibbetts for helping us in the initial steps of the IRAC reduction data. An anonymous referee provided many insightful comments. This publication makes use of data products from Two Micron All Sky Survey, which is a joint project of the University of Massachusetts and the Infrared Processing and Analysis Center, California Institute of Technology. This work is based on observations made with the *Spitzer Space Telescope* (GO-1 0037), which is operated by the Jet Propulsion Laboratory, California Institute of Technology, under a contract with NASA. Support for this work was provided by University of Michigan and NASA grants NAG5-13210, NASA-1277575, and NASA-1285169.

REFERENCES

Abt, H. A., Landolt, A. U., Levy, S. G., & Mochnacki, S. 1976, AJ, 81, 541
Adams, F. C., Hollenbach, D., Laughlin, G., & Gorti, U. 2004, ApJ, 611, 360
Balog, Z., Muzerolle, J., Rieke, G. H., Su, K. Y. L., Young, E. T., & Megeath, S. T. 2007, ApJ, 660, 1532
Baraffe, I., Chabrier, G., Allard, F., & Hauschildt, P. H. 1998, A&A, 337, 403
Barrado y Navascués, D., et al. 2007, ApJ, 664, 481
Bessell, M. S., & Brett, J. M. 1988, PASP, 100, 1134
Briceño, C., Hartmann, L., Hernández, J., Calvet, N., Vivas, A. K., Furesz, G., & Szentgyorgyi, A. 2007, ApJ, 661, 1119
Brown, J. M., Blake, G. A., Qi, C., Dullemond, C. P., & Wilner, D. J. 2008, ApJ, 675, L109
Burningham, B. 2005, Ph.D. thesis, Univ. Exeter
Calvet, N., D'Alessio, P., Hartmann, L., Wilner, D., Walsh, A., & Sitko, M. 2002, ApJ, 568, 1008
Calvet, N., et al. 2005, ApJ, 630, L185
Cardelli, J. A., Clayton, G. C., & Mathis, J. S. 1989, ApJ, 345, 245
Clarke, C. J. 2007, MNRAS, 376, 1350
Carpenter, J. M., Mamajek, E. E., Hillenbrand, L. A., & Meyer, M. R. 2006, ApJ, 651, 49
Chen, C. H., Jura, M., Gordon, K. D., & Blaylock, M. 2005, ApJ, 623, 493
Cieza, L., & Baliber, N. 2007, ApJ, 671, 605
Crowther, P. A. 2007, ARA&A, 45, 177
Currie, T., Kenyon, S. J., Balog, Z., Rieke, G., Bragg, A., & Bromley, B. 2008, ApJ, 672, 558
Dahm, S. E., & Hillenbrand, L. A. 2007, AJ, 133, 2072
D'Alessio, P., Calvet, N., Hartmann, L., Franco-Hernández, R., & Servín, H. 2006, ApJ, 638, 314
D'Alessio, P., Merín, B., Calvet, N., Hartmann, L., & Montesinos, B. 2005a, Rev. Mex. AA, 41, 61
D'Alessio, P., et al. 2005b, ApJ, 621, 461
De Marco, O., & Schmutz, W. 1999, A&A, 345, 163
De Marco, O., Schmutz, W., Crowther, P. A., Hillier, D. J., Dessart, L., de Koter, A., & Schweickhardt, J. 2000, A&A, 358, 187
de Zeeuw, P. T., Hoogerwerf, R., de Bruijne, J. H. J., Brown, A. G. A., & Blaauw, A. 1999, AJ, 117, 354
Dolan, C. J., & Mathieu, R. D. 2002, AJ, 123, 387
Engelbracht, C. W., et al. 2007, PASP, 119, 994
Espaillat, C., Calvet, N., D'Alessio, P., Hernández, J., Qi, C., Hartmann, L., Furlan, E., & Watson, D. M. 2007a, ApJ, 670, L135
Espaillat, C., et al. 2007b, ApJ, 664, L111
Fazio, G. G., et al. 2004, ApJS, 154, 39
Flaherty, K. M., & Muzerolle, J. 2008, AJ, 135, 966
Furlan, E., et al. 2006, ApJS, 165, 568
Gómez, M., & Kenyon, S. J. 2001, AJ, 121, 974
Gordon, K. D., et al. 2005, PASP, 117, 503
Gorlova, N., Balog, Z., Rieke, G. H., Muzerolle, J., Su, K. Y. L., Ivanov, V. D., & Young, E. T. 2007, ApJ, 670, 516
Gorlova, N., Rieke, G. H., Muzerolle, J., Stauffer, J. R., Siegler, N., Young, E. T., & Stansberry, J. H. 2006, ApJ, 649, 1028
Gorlova, N., et al. 2004, ApJS, 154, 448
Gutermuth, R. A., Megeath, S. T., Muzerolle, J., Allen, L. E., Pipher, J. L., Myers, P. C., & Fazio, G. G. 2004, ApJS, 154, 374
Gutermuth, R. A., et al. 2008, ApJ, 674, 336
Haisch, K. E., Lada, E. A., & Lada, C. J. 2001, ApJ, 553, L153
Hartmann, L. 2003, ApJ, 585, 398
———. 2005, in ASP Conf. Ser. 341, Chondrites and the Protoplanetary Disk, ed. A. N. Krot, E. R. D. Scott, & Bo Reipurth (San Francisco: ASP), 131
Hartmann, L., Megeath, S. T., Allen, L., Luhman, K., Calvet, N., D'Alessio, P., Franco-Hernandez, R., & Fazio, G. 2005, ApJ, 629, 881
Hernández, J., Briceño, C., Calvet, N., Hartmann, L., Muzerolle, J., & Quintero, A. 2006, ApJ, 652, 472
Hernández, J., Calvet, N., Hartmann, L., Briceño, C., Sicilia-Aguilar, A., & Berlind, P. 2005, AJ, 129, 856
Hernández, J., et al. 2007a, ApJ, 662, 1067
———. 2007b, ApJ, 671, 1784
Hollenbach, D., & Adams, F. C. 2004, in ASP Conf. Ser. 323, Star Formation in the Interstellar Medium, ed. D. Johnstone (San Francisco: ASP), 3
Houk, N. 1978, Michigan Catalogue for the HD Stars, Vol. 2 (Ann Arbor: Univ. Michigan)
Jeffries, R. D., Pozzo, M., Naylor, T., Harmer, S., & Walter, F. M. 2000, poster paper at ASP Conf. on X-Ray Astronomy 2000
Kenyon, S. J., & Bromley, B. 2005, AJ, 130, 269
Kenyon, S. J., & Hartmann, L. 1995, ApJS, 101, 117
Kharchenko, N. V. 2001, Kinemat. Fiz. Nebesnykh Tel, 17, 409
Lada, C. J., et al. 2006, AJ, 131, 1574
Landsman, W. B. 1993, ASP Conf. Ser. 52, Astronomical Data Analysis Software and Systems II, ed. R. J. Hanisch, R. J. V. Brissenden, & J. Barnes (San Francisco: ASP), 246
Lyra, W., Moitinho, A., van der Bliek, N. S., & Alves, J. 2006, A&A, 453, 101
MacConnell, D. J. 1981, A&AS, 44, 387
Maíz Apellániz, J., Alfaro, E. J., & Sota, A. 2008, in IAU Symp. 250, Massive Stars as Cosmic Engines, ed. André Maeder (Cambridge: Cambridge Univ. Press), in press (arXiv:0804.2553)
Megeath, S. T., Gaidos, E., Hester, J. J., Adams, F. C., Bally, J., Lee, J.-E., & Wolk, S. 2007, preprint (arXiv:0704.1045)
Megeath, S. T., Hartmann, L., Luhman, K. L., & Fazio, G. G. 2005, ApJ, 634, L113
Meyer, M. R., Calvet, N., & Hillenbrand, N. A. 1997, AJ, 114, 288
Millour, F., et al. 2007, A&A, 464, 107
Naylor, T. 1998, MNRAS, 296, 339
Naylor, T., Totten, E. J., Jeffries, R. D., Pozzo, M., Devey, C. R., & Thompson, S. A. 2002, MNRAS, 335, 291
North, J. R., Tuthill, P. G., Tango, W. J., & Davis, J. 2007, MNRAS, 377, 415
Pozzo, M., Jeffries, R. D., Naylor, T., Totten, E. J., Harmer, S., & Kenyon, M. 2000, MNRAS, 313, L23
Reach, W., et al. 2006, Infrared Array Camera Data Handbook, Version 3.0 (Pasadena: Caltech)
Richling, S., & Yorke, H. W. 2000, ApJ, 539, 258

Rieke, G. H., et al. 2004, ApJS, 154, 25
———. 2005, ApJ, 620, 1010
Schaerer, D., Schmutz, W., & Grenon, M. 1997, ApJ, 484, L153
Sicilia-Aguilar, A., et al. 2006, ApJ, 638, 897
Siegler, N., Muzerolle, J., Young, E. T., Rieke, G. H., Mamajek, E. E., Trilling, D. E., Gorlova, N., & Su, K. Y. L. 2007, ApJ, 654, 580
Siess, L., Dufour, E., & Forestini, M. 2000, A&A, 358, 593
Strom, K. M., Strom, S. E., Edwards, S., Cabrit, S., & Skrutskie, M. F. 1989, AJ, 97, 1451
Throop, H. B., & Bally, J. 2005, ApJ, 623, L149
van Leeuwen, F. 2007, A&A, 474, 653